AIAA JOURNAL
Vol. 31, No. 2, February 1993

Structure and Development of Streamwise Vortex Arrays Embedded in a Turbulent Boundary Layer

Bruce J. Wendt* and Isaac Greber†
Case Western Reserve University, Cleveland, Ohio 44106
and
Warren R. Hingst‡
NASA Lewis Research Center, Cleveland, Ohio 44135

The results of an experimental investigation of the structure and development of streamwise vortices embedded in a turbulent boundary layer are presented. Measurements of secondary velocity in the crossplane are used to characterize the vortex array structure. Measurements in the crossplane at two streamwise locations characterize the downstream development of this structure. The initial spacing between vortices is found to strongly influence this development. Enhanced circulation decay is found to occur in arrays of closely spaced vortices. Evidence suggests this decay is due to the merging of neighboring counter-rotating vortex cores.

Nomenclature

c = vortex generator chord length
h = height of vortex generator
N = number of embedded vortices in an array
S = spacing between adjacent vortex generators
U_∞ = freestream velocity
v = normal velocity component
w = spanwise velocity component
x = streamwise coordinate
x_0 = x location of vortex generator trailing edge
y = normal coordinate
y_i = vortex core normal location descriptor
z = spanwise coordinate
z_i = vortex core spanwise location descriptor
α = vortex generator angle of attack
Γ_i = vortex circulation descriptor
δ = boundary-layer thickness
ν = kinematic viscosity
$\omega^i_{\max}$ = vortex peak vorticity descriptor

I. Introduction and Background

A SMALL flow obstruction protruding from a smooth surface will generate a streamwise vortex in much the same way as a trailing vortex is shed from the wing tip of an aircraft. The helical motion of the resulting streamwise vortex, if properly situated with respect to the boundary layer, provides a mixing mechanism capable of energizing the boundary-layer fluid and avoiding or delaying downstream separation. The mixing performance of the vortex depends on the details of the peculiar helical pattern of vortex flow, referred to here as vortex "structure."

The structure of the vortex is most clearly viewed in the crossplane. Following the work of Westphal et al.[1] four descriptors can be identified to quantitatively describe embedded vortex structure in the crossplane. For each embedded vortex i in the array these are as follows.

1) Peak streamwise vorticity: $\omega^i_{\max}$. The peak streamwise vorticity is an indication of vortex concentration. The larger the magnitude of peak vorticity, the thinner and more concentrated the vortex structure.

2-3) The spanwise and normal location of $\omega^i_{\max}$: z_i and y_i. The cross plane location of $\omega^i_{\max}$ corresponds to the center of the vortex, the point around which the vortex "spins."

4) Circulation: Γ_i is a measure of the vortex strength.

The downstream development of this structure, covering a number of test conditions, has been well documented by workers at Stanford University and Imperial College. Eibeck and Eaton[2] and Shabaka et al.[3] have examined the developmental characteristics of the single embedded vortex. The decay of peak vorticity was observed to occur at a rate much greater than the rate of decay of an isolated vortex having the same vortex Reynolds number, Γ_i/ν. Growth and elliptical deformation of the viscous core was observed to accompany the decay of peak vorticity. Westphal et al.[4] have observed that the rate of peak vorticity decay is enhanced by the presence of an adverse streamwise pressure gradient.

The wall imparts a convective motion to the vortex in the cross plane. The single embedded vortex travels along the wall but does not move away from it. This behavior follows what would be expected from a potential model of the vortex, using an image vortex to represent the convective influence of the wall.

The circulation of the single embedded vortex decays slowly with streamwise distance. The decay mechanism originates at the wall where a spanwise component of the wall shear stress gives rise to a torque opposing the rotation of the vortex.

In addition to the influence of the wall and turbulent boundary layer, embedded vortices in array configurations will interact with each other. This interaction modifies their subsequent structural development. The experimental work of Pauley and Eaton[5] documents the development of pairs of counter and corotating vortices. Three types of vortex to vortex interaction were extensively studied: a counter-rotating configuration producing a region of downflow between vortices (a "common downflow" pair); a counter-rotating configuration producing a region of upflow between vortices (a "common upflow" pair); and a pair of corotating vortices.

The streamwise decay of peak vorticity was found to be dependent on the proximity of neighboring vortices. A close

Presented as Paper 92-0551 at the AIAA 30th Aerospace Sciences Meeting, Reno, NV, Jan. 6-9, 1992; received Jan. 28, 1992; revision received Sept. 8, 1992; accepted for publication Sept. 10, 1992.

*Research Associate, Mail Stop: 5-11, 21000 Brookpark Road. Member AIAA.
†Professor, Department of Mechanical and Aerospace Engineering. Associate Fellow AIAA.
‡Aerospace Engineer, Mail Stop 5-11, 21000 Brookpark Road. Member AIAA.

neighbor would strongly perturb and "spread" the vorticity field of an embedded vortex core thereby increasing the rate of decay of peak vorticity beyond levels observed for the single embedded vortex. Vorticity spreading and the rate of peak streamwise vorticity decay were observed to be proportional to the proximity and strength of the neighboring vortex.

Motion of the vortex cores in the cross plane was observed to follow the general characteristics of potential flow theory as outlined by Pearcy.[6] A downflow pair of counter-rotating vortices was observed to push along the wall away from each other. The downflow pair exhibited no tendency to move away from the wall and so the resultant interaction with the boundary layer was strong. An upflow pair of counter-rotating vortices was observed to draw together and convect out of the boundary-layer region. The resultant interaction with the boundary layer was therefore weak. The closer the initial spacing of the vortices, the stronger the tendency toward motion away from the wall. A corotating pair of vortices was observed to merge rapidly into a single embedded vortex. At the downstream measurement station little trace of the original vortex pair was evident in the combined vortex structure.

The streamwise decay of vortex circulation was correlated to the proximity of the vortex to the wall. Circulation decay of vortices in downflow pairs was found to be similar to that exhibited by a single embedded vortex. Circulation decay is reduced for upflow pairs due to the motion of the vortices away from the wall. This behavior, however, could not be validated at the far downstream locations due to the displacement of the vortices outside of the measurement domain.

An upflow pair of counter-rotating vortices in an advanced state of development was the focus of a study by Mehta and Bradshaw.[7] In addition to various mean flow measurements, extensive turbulence data was also obtained.

In this study we have extended the scope of the earlier experiments by examining larger arrays of counter-rotating vortices. The vortex arrays consisted of four embedded vortices produced by a single spanwise row of equally spaced vortex generators. Mean flow measurements of secondary velocity provide the basis for quantifying the structural description of each embedded vortex within an array configuration. A range of initial spacings was examined to comprehensively characterize the influence of vortex to vortex interactions on the downstream development of vortex structure. Cross plane grid resolution (with respect to the scale of the viscous cores) was greater than that found in previous studies. The structure and development of the single embedded vortex was re-examined to take advantage of the higher resolutions employed.

II. Facilities and Procedures

A. Test Facility

This investigation was conducted in the CW-22 test facility at the NASA-Lewis Research Center. The test facility consisted of a subsonic wind tunnel schematically diagrammed in Fig. 1. NASA-Lewis air supply service provided dry air pressurized to 275.8 kPa (40 psig) at the upstream end of the facility, where a valve regulated the airflow into a plenum tank. The large plenum tank aided in reducing the turbulence of the incoming airstream. To further this end, four screens of 34 mesh and 60% porosity were placed at the downstream end of the plenum tank. After exiting these screens the airstream entered a bellmouth contraction where the flow area was reduced by about 60%. The flow then entered a constant area settling chamber and was forced through a 30-cm-thick honeycomb flow straightening grid. Upon leaving the settling chamber the airstream underwent its final contraction to the test section. This contraction section had an inlet to exit area ratio of 6.5 and was designed to make the transition from a flow area of circular geometry, present in the settling chamber, to the octagonal flow area of the test section. Following the test section the airstream entered a transition duct (octagonal to circular) and then to a conical diffuser. After two 90-deg turns

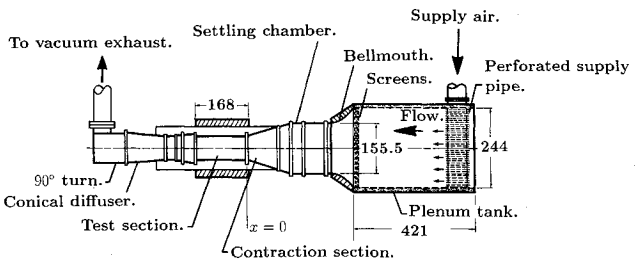

Fig. 1 Schematic diagram of the test facility; all dimensions are in centimeters.

the airstream exited the facility through a valve to the altitude (vacuum) exhaust. At the operational test section Mach number of 0.2 the tunnel mass flow rate was about 21 kg/s. The plenum tank total pressure was maintained at approximately 1 atm and the total temperature was approximately room temperature (15°C, 59°F). For these flow conditions a freestream velocity of about 70 m/s was achieved in the test section.

After a manual startup the operation of the wind tunnel was fully automatic. Pressure and temperature instrumentation located in the plenum tank, settling chamber, and test section provided the data input to set and control tunnel flow conditions. Each flow measuring device, whether operational or research, was monitored by a central minicomputer based operating system.

More information concerning the design and operation of the Mach 1 octagonal wind tunnel may be found in the reports of Refs. 8 and 9.

B. Test Parameters and Research Instrumentation

The flat plate boundary layer was generated inside the test section by means of a vertically mounted splitter plate. Figure 2 shows a cutaway view of the test section with splitter plate mounted. The coordinate system in use is also indicated. The row of vortex generator mounting holes was located 64 cm downstream of the splitter plate leading edge. Here the boundary layer was about a centimeter thick and the Reynolds number was $Re = U_\infty x/\nu \approx 3 \times 10^6$. Boundary layer and five hole pitot probes (with tip diameters of 0.3 and 1.5 mm, respectively) were used to conduct extensive spanwise surveys of the boundary layer in the absence of the vortex generators. This was done at several x locations downstream of the vortex generator mounting station. Velocity profiles consistent with a flat plate turbulent boundary layer were recorded. No spanwise variations in these profiles were detected.

1. Vortex Generator Test Parameters

Each vortex generator was a rectangular fin machined from a single piece of stainless steel stock and having a symmetric cross section. The generators were mounted on the splitter plate surface to produce arrays of counter-rotating vortices. Figure 3a shows the geometry of a typical configuration. The height ratio h/δ and aspect ratio $2h/c$ were maintained at 1.3 for all test conditions examined. Spacing ratios were varied in the range $2.0 \leq S/\delta \leq 7.0$. To produce vortices of equal initial strengths all vortex generators were held at the same magnitude of angle of attack ($\alpha = \pm 10$ deg).

Arrays consisting of four embedded vortices made up the primary set of test conditions. Figure 3b represents the flowfield created by the arrangement of vortex generators in Fig. 3a. In addition to the array configurations, a single embedded vortex (produced by a single vortex generator) was also examined.

2. Velocity Field Study

The velocity structure was determined by traversing the five hole pressure probe in a grid pattern in the (z, y) crossplane. All three components of the mean field velocity vector were

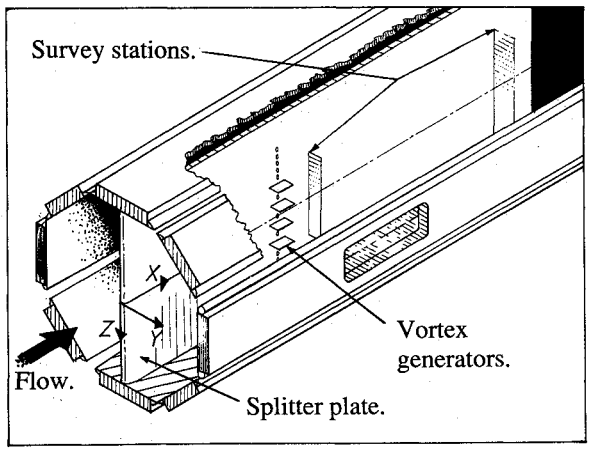

Fig. 2 Cutaway view of the test section showing the splitter plate and coordinate system used.

measured with this probe. The calibration of the five hole probe is outlined in Wendt et al.[10] Since the measured maximum flow angles were relatively small (± 20 deg), the pitch correlation was independent of the yaw angle. Likewise, the yaw correlation was independent of the pitch angle. This behavior was verified during a calibration procedure where it was possible to simultaneously pitch and yaw the probe.

To examine the streamwise development of the vortex arrays crossplane velocity surveys were made at two streamwise locations (x = 74 and 150 cm).

In this study the focus is primarily on the structure of the embedded vortex arrays and the interaction of the arrays with the boundary layer. An important description of this structure lies in the streamwise vorticity field created. This field defines the shape, strength, and extent of the viscous cores. The y extent of the survey grid and the resolution (Δz, Δy) was therefore set to capture and define this vorticity field at each grid location, based on the results of preliminary survey work. A normal extent of 2 cm was sufficient to capture the thin boundary layer and narrow structure of the vortices at the upstream (station 74) crossplane grid. At station 74 Δz = Δy = 0.127 cm. At station 150 the vortex cores were a good deal larger and more diffuse than at station 74. In addition, interaction between vortices in the array could drive the cores away from the wall by as much as several centimeters. Thus, to capture and define the vortex structure at the downstream station, a normal grid extent of at least 4 cm was needed. At station 150 Δz = Δy = 0.203 cm.

The five hole probe was positioned in each crossplane grid by a computer controlled, two axis mechanism.

III. Experimental Results

A. Determination of the Vortex Descriptors

The four structural descriptors of each embedded vortex originate from the secondary velocity data in the crossplane. The velocity field is first converted to a streamwise vorticity field following the relation

$$\omega_x = \left(\frac{\partial w}{\partial y} - \frac{\partial v}{\partial z}\right) \tag{1}$$

Finite difference formulas were used to represent the spatial derivatives in Eq. (1). Figure 4a shows the measured secondary velocity field and corresponding vorticity field of the single embedded vortex at station 74.

The contours of streamwise vorticity define the extent and shape of the viscous core. Opposite signed or "secondary" vorticity is produced at the wall and underneath the vortex by the viscous interaction between the strong spanwise crossflow of the vortex and the wall. This secondary vorticity is convected by the crossflow and collects in the upwash region of the vortex (to the right of the core in Fig. 4a). The region of secondary vorticity tends to grow in size as the vortex develops downstream but rollup of this region into an identifiable vortex structure was not observed in this study.

Evaluation of the structural descriptors proceeds from the vorticity field. The $\omega^i_{\max}$ is located at some grid point having coordinates (z_i, y_i). For the vortex illustrated in Fig. 4a

$$\omega^i_{\max} = 29640\ \text{s}^{-1}, \qquad z_i = 1.52\ \text{cm}, \qquad y_i = 1.02\ \text{cm}$$

The circulation Γ_i was calculated by first isolating the region of core vorticity in the data field, referring to a contour plot such as that included in Fig. 4a. A path enclosing the region of core vorticity and excluding the region of secondary vorticity was then defined. The circulation could then be calculated according to

$$\Gamma_i = \oint_{\text{path}} V \cdot ds \tag{2}$$

where V is the velocity vector in the crossplane and s refers to the path coordinate. By using closed paths composed of line segments in the z or y coordinate directions, the circulation was easily determined. The circulation of the vortex illustrated in Fig. 4a is found to be Γ_i = 0.281 m²/s. It was found that the circulation of the region of induced secondary vorticity was less than about 4% of the corresponding core circulation at station 74, and less than about 10% at station 150.

B. Results at Station 74

In addition to the case of the single embedded vortex, four array test conditions were examined at station 74. Since each array is symmetric with respect to its centerline in the crossplane, only one half of the array was examined. Figures 4b through 4e illustrate the velocity and vorticity structure of the right-hand side (vortices 3 and 4) of the array as the spacing ratio is decreased from 5.0 to 2.0. The corresponding vortex descriptors are listed in Table 1.

Having the structure of the single embedded vortex at station 74 allows us to address the following question: When does the structure of the vortex array become simply a sum of

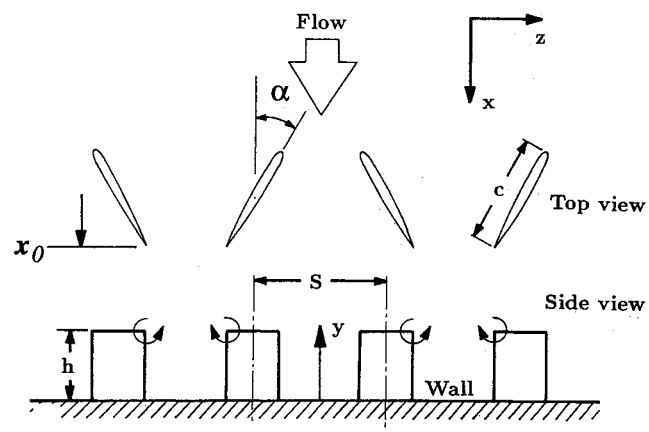

Fig. 3a Geometry of the vortex generator array.

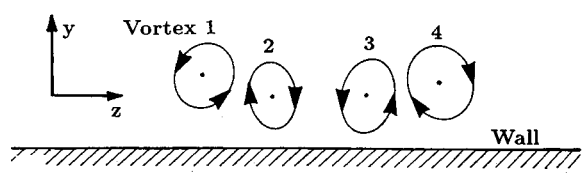

Fig. 3b Resultant vortices downstream of the vortex generator array, viewed in the crossplane.

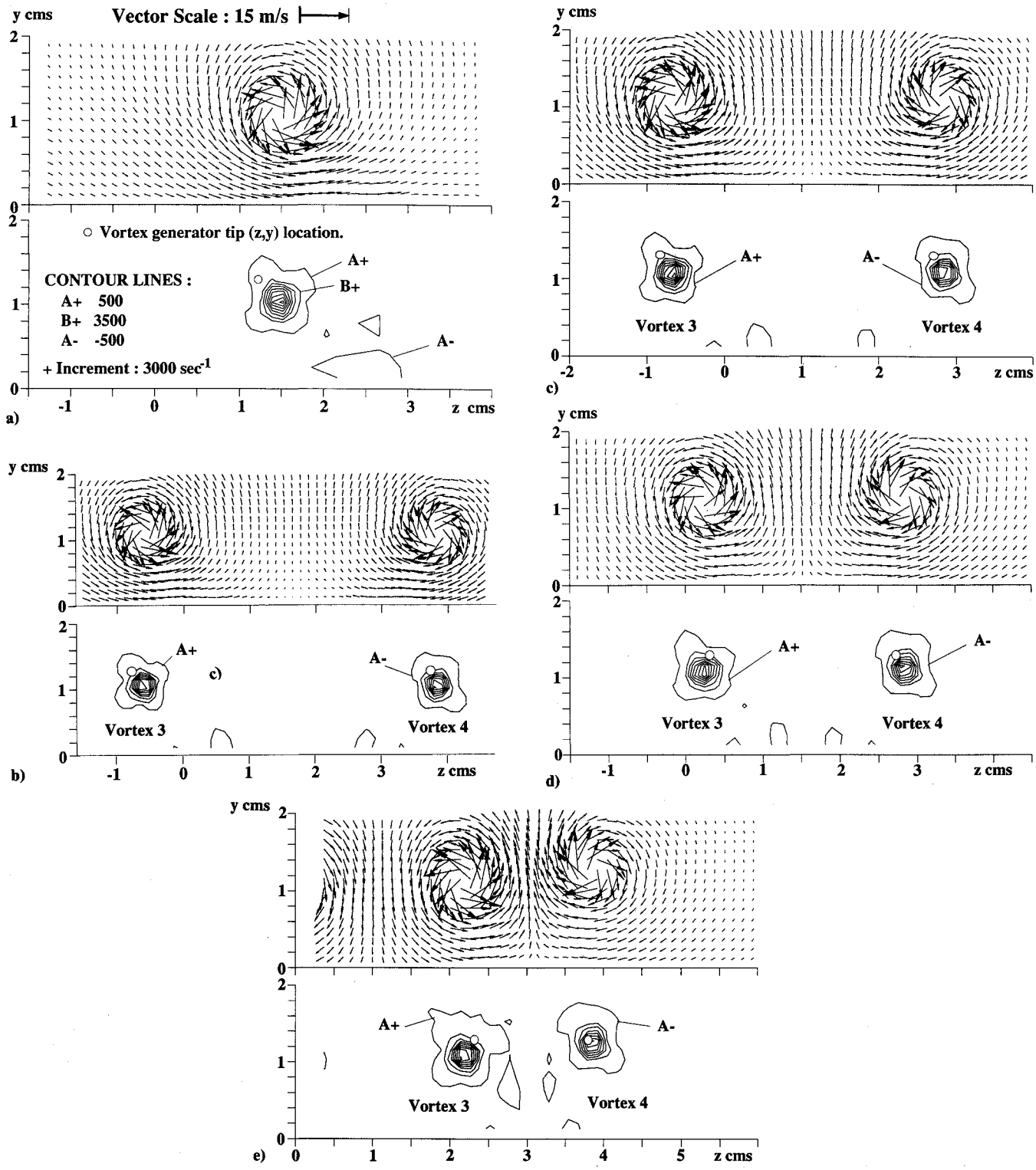

Fig. 4 Measured secondary velocities (vector plots) and streamwise vorticities (contour plots) at station 74: a) single embedded vortex, b) spacing ratio 5.0 test case, c) spacing ratio 4.0 test case, d) spacing ratio 3.0 test case, and e) spacing ratio 2.0 test case.

vortices whose individual structure is identical to the single embedded vortex? Naturally, this behavior is expected when the distance between vortices is large enough. Consider Fig. 4b which shows the initial spacing ratio 5.0 array. Vortex 3 clearly is similar in appearance and structure to the single embedded vortex in Fig. 4a. Vortex 4 is merely its mirror image. Figures 4c–4e reveal a similar pattern. The velocity vector and vorticity patterns indicate the vortex retains its circular core shape regardless of the distance between vortices. Apparently each vortex is so strongly condensed that its shape can withstand the distortional convective forces of its neighbors. This holds true even at the smallest initial spacing ratio, $S/\delta = 2.0$, shown in Fig. 4e. Here, vortex 3 is crowded by neighboring vortices in close proximity on both sides, vortex 4 to the right, and vortex 2, visible to the left, and just out of the survey grid.

C. Results at Station 150

Figures 5a–5g illustrate the vortex structures found at the downstream station. Figure 5a illustrates the velocity and vorticity structure of the single embedded vortex and Figs. 5b–5g illustrate the structure of the four element arrays with initial spacing ratios from 7.0 to 2.0. The vortex descriptors corresponding to each test case are listed in Table 2.

By comparing Figs. 4a and 5a we note the general differences in vortex structure between the upstream and downstream stations. At the downstream station the vortex core has increased considerably in size but is now much more diffuse. The ω^i_{max} is reduced to about 5% of its value at station 74. Peak secondary velocities in the vicinity of the core have decreased from a magnitude of about 18 m/s at station 74 to about 5 m/s at station 150. The wall has convected the core roughly 3 cm to the right from its point of origin in the crossplane. The sustained convection by the strong crossflow underneath the vortex has created an extensive region of secondary vorticity in the upwash region of the vortex, to the right of the vortex core in Fig. 5a. The vorticity profile of the vortex core is also affected by the convection of this crossflow. Note how the core profile contours are flattened into an elliptical shape following the wall in Fig. 5a.

Table 1 Vortex descriptors at station 74

S/δ	Vortex no.	Γ_i, m²/s	ω^i_{max}, s^{-1}	z_i, cm	y_i, cm
Single	1	0.281	29,640	1.52	1.02
2.0	3	0.287	27,800	2.14	1.02
	4	−0.266	−26,060	3.79	1.27
3.0	3	0.269	27,750	0.25	1.02
	4	−0.262	−25,860	2.79	1.14
4.0	3	0.280	30,280	−0.64	1.02
	4	−0.262	−23,810	2.79	1.14
5.0	3	0.279	27,880	−0.64	1.02
	4	−0.268	−25,500	3.81	1.02

The embedded vortices in array configurations exhibit some of the same qualitative developmental characteristics found in the case of the single embedded vortex described earlier. However, if we compare the upstream and downstream vortex descriptors from one test case to another we find that the developmental trends of vortex structure in array configurations also depend strongly on the initial spacing of the vortices.

Vortex trajectories are determined by the convective effects of wall and neighboring vortices. The larger spacings produce vortices that travel along the wall to form widely spaced upflow pairs at the downstream crossplane. This behavior is evident in Figs. 5b and 5c (S/δ = 7.0 and 6.0, respectively). As the initial spacing ratio of the generators is decreased the strength of the upflow pairing is increased and displacement

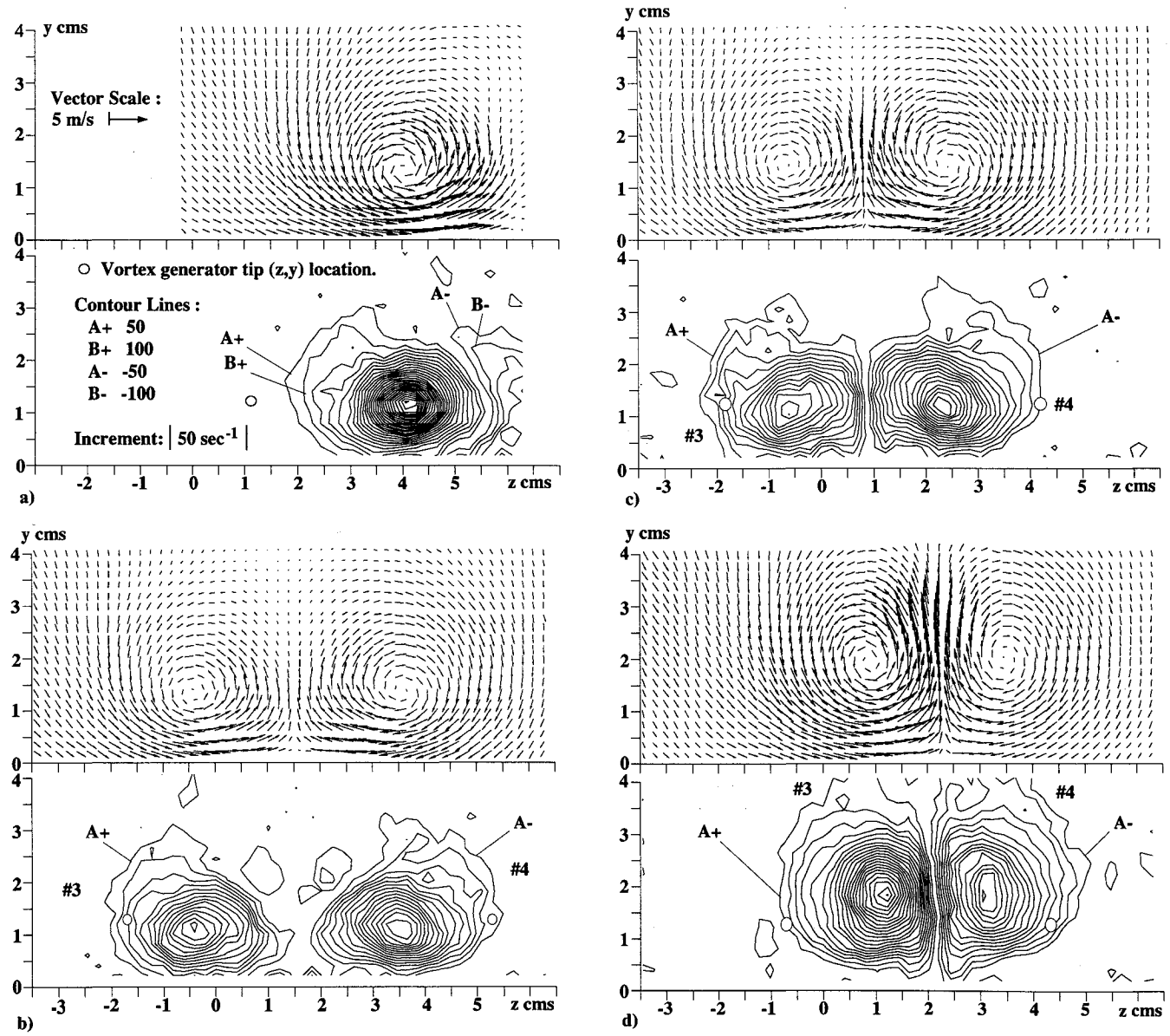

Fig. 5 Measured secondary velocities (vector plots) and streamwise vorticities (contour plots) at station 150: a) single embedded vortex, b) spacing ratio 7.0 test case, c) spacing ratio 6.0 test case, and d) spacing ratio 5.0 test case.

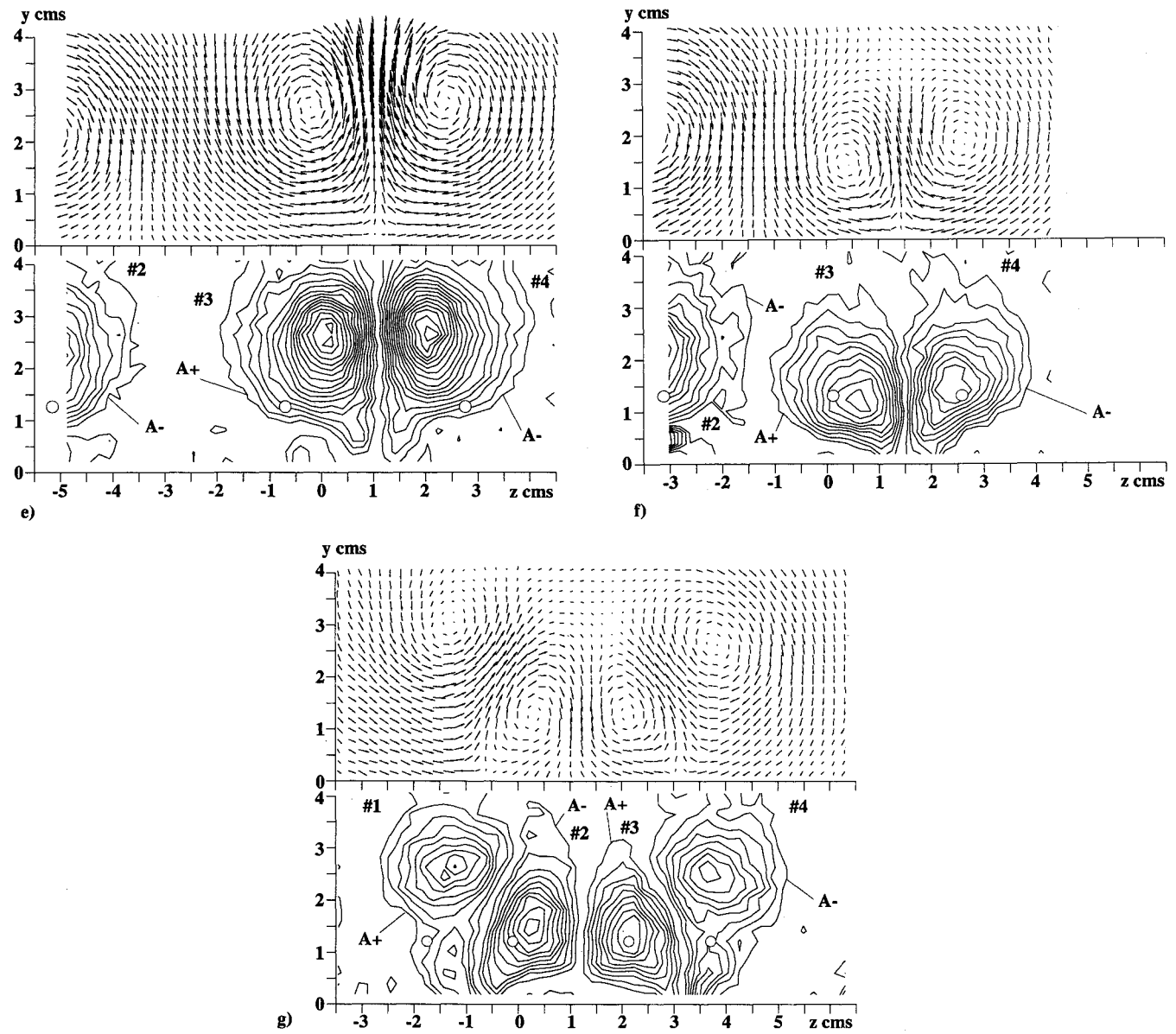

Fig. 5 (continued) Measured secondary velocities (vector plots) and streamwise vorticities (contour plots) at station 150: e) spacing ratio 4.0 test case, f) spacing ratio 3.0 test case, and g) spacing ratio 2.0 test case.

of the pair from the wall becomes more pronounced at the downstream grid (Figs. 5d and 5e). This trend does not continue through to the smallest spacings examined, as is commonly assumed. At a spacing ratio of 3.0 the motion of the upflow pair away from the wall is hindered by the nearby presence of the other upflow pair in the array. At a spacing ratio of 2.0 the array at the downstream station ceases to be a summation of upflow pairs. The array now consists of one strong downflow pair created by the proximity of the interior vortices 2 and 3, with the exterior vortices 1 and 4 pushing up on either side of the array. Figures 5f and 5g indicate the behavior of the array at these smaller values of S/δ.

The downstream values of peak vorticity indicate that the decay of this quantity depends partly on the proximity and strength of neighboring vortices. Decay is enhanced with increased neighbor proximity and strength. This effect, termed "vorticity spreading," was first noticed in pairs of embedded vortices by the Stanford workers Pauley and Eaton.[5]

Figure 6 is a plot of circulation magnitude at station 150, averaged over all four vortices in the array, vs initial spacing ratio. The decay of vortex circulation for vortices in arrays produced with large initial spacings is similar in extent to that exhibited by the single embedded vortex. The effects of wall friction are assumed to be responsible. For vortices in arrays produced with intermediate initial spacings, motion away from the wall decreases the circulation losses somewhat. Large losses in circulation occur for vortices produced at spacing ratios of 2.0 and 3.0. The vortices in these arrays are no closer to the wall than the single embedded vortex. This leads us to conclude that wall friction effects alone cannot explain the large losses in circulation occurring for vortices in these arrays. Just what mechanism accounts for this circulation loss? The evidence provided by the crossplane plots at both survey grids suggests that a cancellation or merging effect is occurring between the closely spaced opposite signed cores in the arrays with $S/\delta = 2.0$ and 3.0.

It is often assumed that equally spaced arrays of vortex generators set in a counter-rotating configuration produce vortices which tend to lift out of the boundary layer quickly, thereby reducing or eliminating the benefits of vortical mixing on the boundary layer. Whereas this is true for intermediate values of the spacing ratio, it does not hold true for tighter spacings. Tight arrays of counter-rotating vortices are confined to the vicinity of the boundary layer. Increased mixing performance may result simply because the number of embedded vortices per unit span length is increased. The downstream distance to which this beneficial mixing performance is achieved will be limited due to the rapid attenuation of indi-

Table 2 Vortex descriptors at station 150

S/δ	Vortex no.	Γ_i, m²/s	ω^i_{max}, s^{-1}	z_i, cm	y_i, cm
Single	1	0.228	1440	4.06	1.22
7.0	3	0.201	726	−0.41	1.22
	4	−0.206	−774	3.66	1.02
6.0	3	0.207	693	−0.61	1.02
	4	−0.217	−902	2.24	1.22
5.0	3	0.239	1170	1.22	1.83
	4	−0.221	−792	3.05	1.83
4.0	2	−0.223	−739	−5.49	2.44
	3	0.227	857	0.20	2.84
	4	−0.228	−902	2.03	2.64
3.0	3	0.151	536	2.84	1.02
	4	−0.146	−515	4.47	1.22
2.0	1	0.112	471	−1.22	2.64
	2	−0.104	−554	0.20	1.42
	3	0.100	527	2.24	1.02
	4	−0.120	−422	3.66	2.44

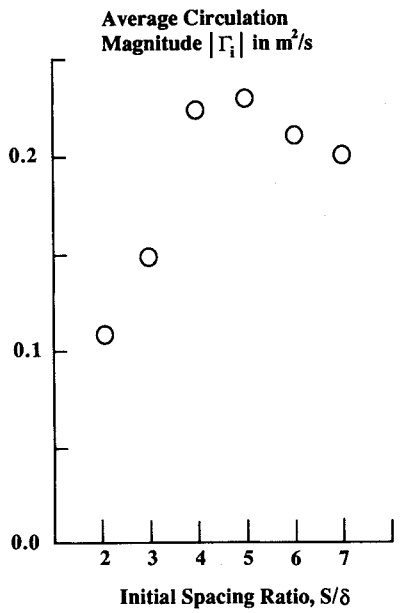

Fig. 6 Average circulation magnitude at station 150 vs initial spacing ratio.

vidual vortex strength. In many applications, such as on airfoils or in diffusers, there is no need to maximize this distance; rather, the important requirement is that separation is avoided at certain critical locations. Tight arrays of vortex generators mounted just upstream of such locations may then provide the greatest mixing benefits.

IV. Conclusions

An experimental investigation of the structure and development of streamwise vortex arrays embedded in a turbulent boundary layer was conducted. The vortices were generated by a single spanwise row of rectangular vortex generator blades mounted on the surface of a vertical splitter plate installed inside the test section of a subsonic wind tunnel.

Measurements of the secondary velocity field in the crossplane provided the basis for characterization of vortex structure. Vortex structure was characterized by four descriptors. The center of each vortex was located at the spanwise and normal position of peak streamwise vorticity. Vortex concentration was characterized by the magnitude of peak streamwise vorticity and the vortex strength by its circulation.

Measurements of the velocity field were conducted at two crossplane locations to examine the streamwise development of the vortex arrays. The developmental trends inferred from the experimental results at the upstream and downstream cross planes depend strongly on the initial spacing of the vortex generators.

1) Large spacings produce vortices that travel along the wall to form arrays consisting of widely spaced upflow pairs. The vortices in these upflow pairs move away from the wall region. Motion away from the wall weakens the interaction between the vortex array and the boundary layer. These vortices retain much of their original strength due to the reduction in circulation losses from wall friction effects.

2) Small spacings produce tight arrays of weak vortices that remain in close proximity to the wall. The resultant interaction with the boundary layer is strong. Large losses in individual vortex strength indicate a circulation loss mechanism in addition to wall friction effects. Profiles of streamwise vorticity show that the counter-rotating cores are merging together as they develop downstream.

Acknowledgment

The support of NASA-Lewis Research Center under grant NAG 3-520 is gratefully acknowledged by the authors.

References

[1]Westphal, R. V., Pauley, W. R., and Eaton, J. K., "Interaction Between a Vortex and a Turbulent Boundary Layer in a Streamwise Pressure Gradient," *Fifth Symposium on Turbulent Shear Flows,* Pennsylvania State Univ., University Park, PA, 1985, pp. 7.1–7.8.

[2]Eibeck, P. A., and Eaton, J. K., "An Experimental Investigation of the Heat-Transfer Effects of a Longitudinal Vortex Embedded in a Turbulent Boundary Layer," Stanford Univ., Rept. MD-48, Stanford, CA, Nov. 1985.

[3]Shabaka, I. M. M. A, Mehta, R. D., and Bradshaw, P., "Longitudinal Vortices Imbedded in Turbulent Boundary Layers, Part 1. Single Vortex," *Journal of Fluid Mechanics,* Vol. 155, June 1985, pp. 37–57.

[4]Westphal, R. V., Pauley, W. R., and Eaton, J. K., "Interaction Between a Vortex and a Turbulent Boundary Layer, Part 1: Mean Flow Evolution and Turbulence Properties," NASA TM 88361, Jan. 1987.

[5]Pauley, W. R., and Eaton, J. K., "The Fluid Dynamics and Heat Transfer Effects of Streamwise Vortices Embedded in a Turbulent Boundary Layer," Stanford Univ., Rept. MD-51, Stanford, CA, Aug. 1988.

[6]Pearcy, H. H., "Shock Induced Separation and its Prevention by Design and Boundary Layer Control," *Boundary Layer and Flow Control, Its Principles and Applications,* 1st ed., Vol. 2, Pergamon Press, New York, 1961, pp. 1166–1344.

[7]Mehta, R. D., and Bradshaw, P., "Longitudinal Vortices Imbedded in Turbulent Boundary Layers, Part 2: Vortex Pair with Common Flow Upwards," *Journal of Fluid Mechanics,* Vol. 188, March 1988, pp. 529–546.

[8]Harrington, D. E., Burley, R. R., and Corban, R. R., "Experimental Evaluation of Wall Mach Number Distributions of the Octagonal Test Section Proposed for NASA Lewis Research Center's Altitude Wind Tunnel," NASA TP 2666, Nov. 1986.

[9]Burley, R. R., and Harrington, D. E., "Experimental Evaluation of Honeycomb/Screen Configurations and Short Contraction Section for NASA Lewis Research Center's Altitude Wind Tunnel," NASA TP 2692, July 1987.

[10]Wendt, B. J., Greber, I., and Hingst, W. R., "The Structure and Development of Streamwise Vortex Arrays Embedded in a Turbulent Boundary Layer," NASA TM 105211, Sept. 1991.